A method for determining the ductile damage parameters of high strength steels and weld metal

Xu Wang[1,2], Jian Shuai[1], Wei Ren[1], Tieyao Zhang[1], Jianying He[2] and Zhiliang Zhang[2]

Abstract
The microvoid based Gurson-Tvergaard-Needleman (GTN) model is a powerful tool for predicting ductile fracture behavior, and application of such model to steels and welds needs the identification of microvoid related damage parameters. Currently, there is no standard damage parameter identification method available. In this study the previously proposed complete Gurson model (CGM) where a physical void coalescence mechanism is incorporated into the GTN model is revisited. According to the CGM, the void nucleation process dictates ductile fracture. By adopting the cluster nucleation model with an effective initial void volume fraction as the only controlling parameter, a method is proposed to explicitly determine the effective initial void volume fraction from the strain at maximum load and strain at fracture of a specially designed notched tensile specimen. The proposed equation has been experimentally verified by applying to three high strength materials, including a X80 pipeline steel and associated weld metal, and a 15CrMo steel. A general procedure for damage parameter identification is also suggested. It is argued that the obtained effective initial void volume fraction can be treated as a type of material ductility indicator.

Keywords
complete Gurson model (CGM), initial void volume fraction, damage parameter identification, notched tensile specimen, weldment

Introduction

Structural components made of high strength steels may fail by ductile fracture. It is well recognized that ductile fracture of steels results from the nucleation, growth and coalescence of microvoids. The most widely used model for ductile fracture was originally developed by Gurson (1977), and further modified and improved by Tvergaard and Needleman (Tvergaard, 1981, 1982; Tvergaard and Needleman, 1984). The application of this ductile damage model, also well-known as the GTN model, needs the identification of as many as 17 parameters (Zhang et al., 2018), including the material-specific void (nucleation and coalescence) parameters, constitutive parameters, characteristic length parameter(s) as well as other material-independent model parameters. It is a common practice to calibrate the parameters of the GTN model through a combination of experiments and numerical simulations (Sun et al., 1989; Springmann and Kuna, 2005; Abendroth and Kuna, 2006; Seupel et al., 2020; Miloud et al., 2019). Smooth and notched tensile specimens where the stress/

strain gradients were not strong and finite element mesh size does not play a significant role, are often used to determine the void parameters (Zhang et al., 2000). When the GTN model is applied to cracked components where severe stress gradient exists in the vicinity of crack tip, the predicted failure becomes mesh size dependent. In such cases, a so-called non-local characteristic length parameter(s) should be considered (Zhang et al., 2018). Fracture mechanics specimens such as compact tension (Acharyya and Dhar, 2008; Dotta and Ruggieri, 2004) single edge notched tension (Chen and Lambert, 2003), single edge

[1]College of Safety and Ocean Engineering, China University of Petroleum, Beijing, China
[2]Department of Structural Engineering, Norwegian University of Science and Technology (NTNU), Trondheim, Norway

Corresponding author:
Zhiliang Zhang, Norwegian University of Science and Technology Faculty of Engineering, Structural Engineering, Richard Birkelands vei 1A, Trondheim, Norway.
Email: zhiliang.zhang@ntnu.no

notched bending (Qiang and Wang, 2019; Sarzosa et al., 2016), drop weight tear testing (Scheider et al., 2014; Nonn and Kalwa, 2012) have been used for the calibration of both the void and characteristic length parameters either separately or simultaneously. It is interesting to note that machine learning methods have also been recently applied to the identification of GTN parameters (Chen et al., 2021; Ouladbrahim et al., 2021). In order to limit the scope, this study will focus only on the void parameters.

As far as void parameters concerned, it has been noted by Zhang (1996) more than two decades ago that when comparing with a set of experimental results, the fitted GTN damage parameters are not unique. This non-uniqueness problem implies that different combinations of void nucleation and coalescence parameters may lead to indistinguishable macroscopic responses. This non-uniqueness problem may not have severe consequence if the purpose is to simulate the macroscopic behavior of a specific structural component. However, it does have serious implications in terms of the physical interpretation, transferability of the void parameters and classification of materials deformation and fracture behavior based on damage parameters.

The non-uniqueness problem partly attributes to the lack of a physical void coalescence mechanism in the GTN model which treats the void nucleation and coalescence as two independent events. As a viable solution to the problem, by incorporating a physical void coalescence mechanism based on Thomason's plastic limit load model (Thomason, 1990) into the GTN model, a so-called complete Gurson model (CGM) has been proposed by Zhang (Zhang et al., 2000). The key feature of the CGM is that the void coalescence is a natural result of the plastic deformation of a material with nucleated voids, and the so-called critical void volume fraction at the beginning of coalescence f_c, is thus not a material constant and does not need to be fitted or settled beforehand. The great advantage of the CGM is that in specimens where the stress/strain gradients are not significant, ductile fracture is solely controlled by the void nucleation process. If the ductile fracture behavior of these specimens is known experimentally, the void nucleation parameters can be inversely determined from the measured load-displacement curves.

In the literature, it has been a common practice to estimate the initial volume fraction f_0, from the volume fraction of primary particles such as MnS in steels (Tanguy and Besson, 2002; Tanguy et al., 2005). However, the problem is that normally not every particle, and only an unknown fraction of these particles will nucleate voids during the plastic deformation. In this study, we hypothesize that the initial void volume fraction can be obtained inversely through tests and simulations. By adopting the cluster nucleation model and assuming that the void

nucleation is represented by an effective initial void volume fraction, in this paper, the CGM is applied to study the relationship between the inputted f_0 and the tensile properties of a specially designed notched tensile specimen for the purpose to develop a method for inversely determining the f_0.

In the following, Section 2 briefly revisits the CGM. Section 3 describes the specially designed notched tensile specimen used. In Section 4, the numerical simulation procedure, the correlation data and the obtained equation to explicitly calculate the f_0 are presented. The proposed equation is experimentally verified by applying to three engineering materials with different plastic strain hardening ability and ductility, including a high strength pipeline steel X80, a X80 associated weld metal and a 15CrMo steel. A recommended procedure for determining the f_0 is suggested. Potential to treat the obtained the f_0 as a ductility indicator and use the f_0 to classify the deformation and fracture behavior of steels and welds together with suggested future work and main conclusions are presented in Section 5.

Revisit of the complete Gurson model

The special feature of the complete Gurson model is the introduction of a physically based coalescence criterion. In the following the GTN (Gurson, 1977; Tvergaard, 1981, 1982; Tvergaard and Needleman, 1984) model will be introduced first. The GTN model describes the homogeneous yielding and void growth behavior of a unit cell with a void located in the centre. The yielding function is expressed as:

$$\phi\left(q, \overline{\sigma}, f, \sigma_m\right) = \frac{q^2}{\overline{\sigma}^2} + 2q_1 f \cosh\left(\frac{3q_2\sigma_h}{2\overline{\sigma}}\right) - 1 - (q_1 f)^2 = 0 \quad (1)$$

where q is the von Mises stress, σ_h is the mean stress, $\overline{\sigma}$ is the flow stress, f is the current void volume fraction. q_1 and q_2 are constants introduced by Tvergaard, 1981, 1982 to modify the Gurson model. Fixed values of $q_1 = 1.5$ and $q_2 = 1.0$ have been used in this study.

The application of the GTN model requires the information about the void nucleation process. In general, void nucleation can be cluster-based or of statistical nature (Zhang et al., 2000). The cluster model which usually assumes that the micro-voids are nucleated upon the onset of plastic deformation, is one of the most commonly used models to describe void nucleation for ductile metals. The cluster nucleation model is adopted in this work. The advantage of the cluster void nucleation model is that there is only one controlling parameter, namely the initial void volume fraction f_0. The growth of existing voids can be expressed by assuming that the matrix material is incompressible,

$$df = (1 - f)d\boldsymbol{\varepsilon}^P : \mathbf{I} \qquad (2)$$

where $\boldsymbol{\varepsilon}^P$ is the plastic strain tensor, $\mathbf{I}$ is the second-order unit tensor. When the void volume fraction f grows to a critical value, f_c, void coalescence occurs. Once the void coalescence has started, Tvergaard and Needleman (1984) introduced a function to simulate the process of void coalescence by accelerating the void growth:

$$f^* = \begin{cases} f & \text{for } f \leq f_c \\ f_c + \dfrac{f_u^* - f_c}{f_F - f}(f - f_c) & \text{for } f > f_c \end{cases} \qquad (3)$$

where $f_u^* = 1/q_1$. When $f > f_c$, f is replaced by f^* in equation (1). When f reaches the failure volume fraction f_F, the void coalescence ends. It has been shown that the minimum value of f_F is close to 0.15 and an approximation $f_F = 0.15 + 2f_0$ has been proposed by (Zhang et al., 2000). In most of the literature, an arbitrary or fitted constant f_c has been used and no physical coalescence criterion is considered. (Thomason, 1990) proposed a physically-based plastic limit load model to describe void coalescence. Once the void coalescence mechanism is implemented, the void coalescence is thus a result of the competition between the homogeneous deformation mode described by the GTN model and localized deformation mode governed by the plastic limit load model (Zhang and Niemi, 1994a).

By incorporating the GTN model for void growth and Thomason's plastic limit load model for void coalescence, the CGM is obtained. It is called "complete" in a sense that once the void nucleation process is known, the CGM now can physically capture the complete void growth and coalescence process without a need of using any artificial void coalescence criterion or constant (Zhang and Niemi, 1994a, 1994b). It is worth emphasizing that in the CGM void coalescence is not determined by the so-called critical void volume fraction f_c. With the CGM and in the absence of stress/strain gradient, ductile failure is intrinsically controlled by the void nucleation. The CGM has been implemented into the ABAQUS using a user subroutine UMAT developed by Zhang with dedicated efficient numerical integration algorithms (Zhang, 1995a, 1995b; Zhang and Niemi, 1995), a free copy of the UMAT source code for the implementation can be obtained from the corresponding author.

It must be noted that the CGM treats the voids from the nucleation to the end of coalescence as spherical and the void shape change during the plastic deformation is not considered. The interaction between the voids is also neglected. Thomason's plastic limit load model is not the only one which can be used for describing void coalescence. Other sophisticated coalescence models which consider both plasticity and void anisotropy can be found in (Benzerga and Leblond, 2010).

The "magic" notched tensile specimen for determining both the stress-strain curve and damage parameters

Standard tensile bar specimen used for determining materials' stress-strain curve has several limitations in terms of the size of specimen required, unpredictable necking position and the need to perform Bridgman correction (Zhang et al., 2002). Notched round bar tensile specimens are good alternatives to the conventional smooth tensile specimen for characterizing material tensile properties. Notched tensile specimens possess several advantages compared with the smooth one. Firstly, unlike the smooth specimen where necking often occurs in a random manner, the necking in the notched specimens always appear at the intended location. This is especially appealing for the case when the volume of the material to be tested is too small for machining a standard tensile specimen, for example the heat affected zone or weld metal in a steel weldment. Secondly, recent studies show that material's plastic flow stress-strain curve can be conveniently obtained from notched tensile specimens. In particular, there exists a "magic" notched tensile specimen (Tu et al., 2017), from which the load-minimum cross-sectional area reduction curve recorded can be directly converted to material's equivalent stress-strain or plastic flow stress-strain curve without the need of performing the non-trivial Bridgman correction (Tu et al., 2017, 2018, 2019, 2020).

For a general notched round bar tensile specimen sketched in Figure 1(a), L and D_0 are the initial length and diameter, a_0 is initial radius of minimum cross section, R_0 is initial radius of the notch. Zone W and Zone B are used to distinguish the weld and base metal of a weldment, and H is the width of the weld metal. Early studies have shown that when H is larger than $0.5\,D_0$, the properties of the Zone B will not influence the results of the measured weld metal properties (Tu et al., 2017, 2018, 2020). The average true strain of a notched tensile bar specimen is calculated from the reduction in the minimum cross-sectional area: $\varepsilon_t = 2\ln(a_0/a)$, where ε_t is the average true strain, a is the current radius of minimum cross section. The average engineering stress and true stress of a notched tensile specimen are calculated by the applied load divided by the respective initial and current minimum cross-sectional area, $\sigma_e = P/(\pi a_0^2)$ and $\sigma_t = P/(\pi a^2)$ where σ_e is the engineering stress, σ_t the true stress, P is applied load. The engineering stress at the maximum load is marked as σ_m, and the true stress at fracture is denoted as σ_f. The true strains corresponding to σ_m and σ_f are marked as ε_m and ε_f, respectively.

The ratio of minimum cross section radius to notch radius, a_0/R_0 is a key characteristic of the notched tensile specimen. Our previous studies have shown that among all the notched specimens, there is one "magic" notch geometry, $a_0/R_0 = 2$, which possesses a special feature. It was found that by normalizing the true stress of the "magic" notched tensile specimen by a geometry factor $G^m = -0.824n + 1.6189$, where n is the plastic strain hardening exponent and can be
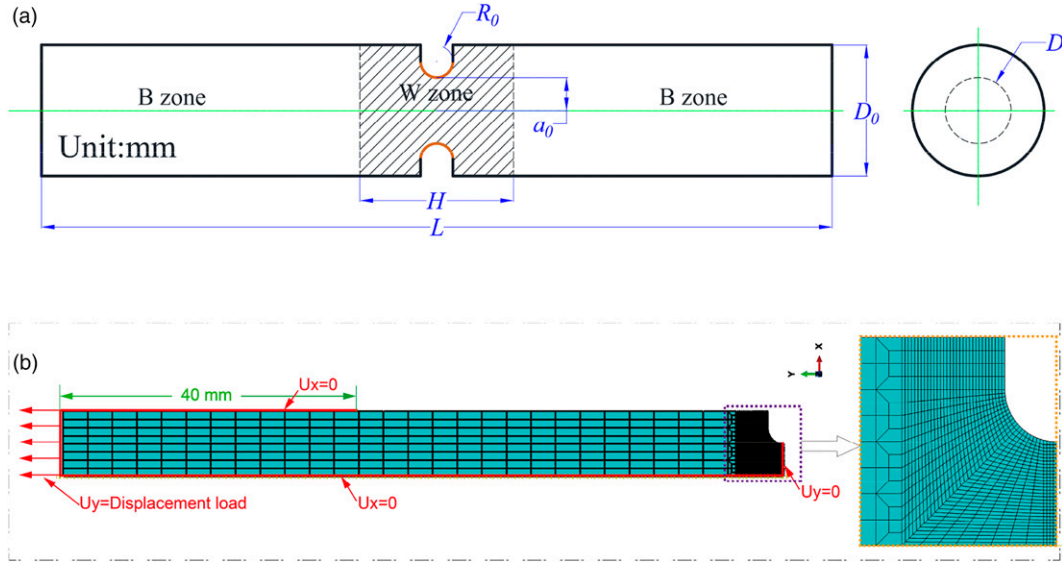
Figure 1. (a) The geometry of the round notched bar specimen used in the numerical analyses and experimental verification, (b) The finite element mesh and boundary conditions used.

approximated by the strain at the maximum load ε_m, the normalized true stress – true strain curve outputted from the notched specimen, $\frac{\sigma_t}{G^m} - \varepsilon_t$, represents the equivalent stress-strain relation of the material. Details about the "magic" notched tensile method can be found in (Tu et al., 2017, 2018, 2019, 2020). In this study, $L = 180$ mm, $D_0 = 16$ mm, $a_0 = 4$ mm and $R_0 = 2$ mm have been used in both the numerical simulation and experiments.

Inversely determining the initial void volume fraction

In the following we apply the CGM to analyze the "magic" notched tensile specimen made of materials with different plastic hardening exponents to generate the correlation data between the fracture strain and inputted initial void volume fraction. An explicit equation will be derived to inversely calculate the initial volume fraction from the data points. The obtained initial void volume fraction will then be applied to compare the predicted fracture strains with the experimental values. A recommended procedure to utilize the method for parameter identification is also suggested.

The numerical procedure

In order to establish the correlation between the inputted damage parameters and the predicted fracture strain, a 1/4 of the axisymmetric notched specimen was modeled with CAX4 element in ABAQUS, as shown in Figure 1(b). The fracture strain was calculated from the predicted cross-sectional area reduction at failure using the CGM. A remote homogenous displacement (clamped boundary condition)

was applied at the end of the specimens. The NLGEOM option was activated to take the large-strain effect into account. A general power-law plastic hardening model was used in the parametric study:

$$\overline{\sigma} = \sigma_0 \left(1 + \frac{\varepsilon_p}{\varepsilon_0} \right)^n \tag{4}$$

where $\overline{\sigma}$ is the flow stress, σ_0 is the yield stress, ε_p is the equivalent plastic strain, ε_0 is the yield strain, n is the strain hardening exponent. In all the analyses, Young's modulus $E = 210$ GPa and Poisson ratio $v = 0.3$ have been applied. Strain hardening exponent n from 0.02 to 0.2 and the initial void volume fraction f_0 in the range from 0.000,001 to 0.01 have been analyzed. The yield stress σ_0 varied from 400 to 1000 MPa, however, it can be expected that the yield stress does not have a remarkable influence on the predicted fracture strain. Because the notch induces a stress concentration, the influence of element size on the ductile fracture needs to be assessed.

The local element size along the middle section was set as l_0, and a transition mesh was used to bridge the fine and coarse mesh. A range of finite element size from 0.05 mm to 0.5 mm was analyzed. Some preliminary analyses show that the range of element size utilized does not have any visible effect on the load-displacement curves of the notched tensile specimen until the fracture point. It can also be noted that the element size used does not noticeably influence the true strain at the maximum load, ε_m. The general observation is that the larger the element size, the larger the resulted fracture strain. In order to better illustrate the effect of mesh size, the fracture strain versus normalized element size is plotted in 2a for constant $f_0 = 0.0001$ and Figure 2(b) for constant

hardening exponent n. Figure 2 shows that when the element size is large, the fracture strains in both cases with constant n and constant f_0 are an increasing function of the mesh size. When the element size is small enough, for example, when a_0/l_0 is larger than 20, the fracture strain is practically independent of the element size. Based on these observations, a default value of $a_0/l_0 = 40$ ($l_0 = 0.1$ mm) has been used in the following analyses unless indicated otherwise.

The correlation data and explicit equation

When the CGM is used, the fracture strain of the notched tensile specimen depends on two key factors, the plastic strain hardening exponent n and initial void volume fraction f_0. For the given notch geometry, the fracture strain ε_f can be expressed as follows:

$$\varepsilon_f = \varepsilon_f(n, f_0) \tag{5}$$

where the fracture strain ε_f and the plastic hardening exponent (strain at the maximum load) $n = \varepsilon_m$ can be obtained directly from the notched tensile test.

Figure 3(a) shows the predicted fracture strain vs the strain hardening exponent n for the cases with f_0 in the range 10^{-6}–10^{-2}, which should cover most of the engineering materials. It is interesting to note that for a given value of f_0, fracture strain ε_f increases approximately in a linear manner with the hardening exponent n. The relationship between the initial void volume fraction f_0 and the fracture strain ε_f is shown in Figure 3(b) with n in the range from 0.02 to 0.2. As f_0 increases from 10^{-6} to 10^{-3}, the ε_f decreases drastically, and the decrease slows down to a nearly linear manner when f_0 is larger than 10^{-3}.
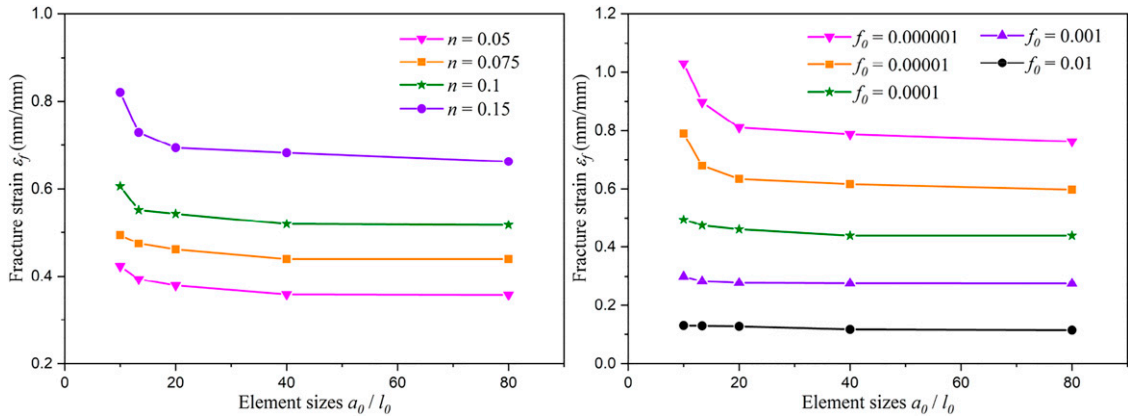

Figure 2. Influence of finite element size on the predicted fracture strain by CGM model, (a) for the cases with a fixed $f_0 = 0.0001$ and varying degrees of strain hardening, and (b) for the cases with fixed hardening exponent $n = 0.075$ and different initial void volume fractions. The yield stress in both cases is fixed as $\sigma_0 = 555$MPa. The default element size, $a_0/l_0 = 40$ and the "magic" notched tensile specimen were used.
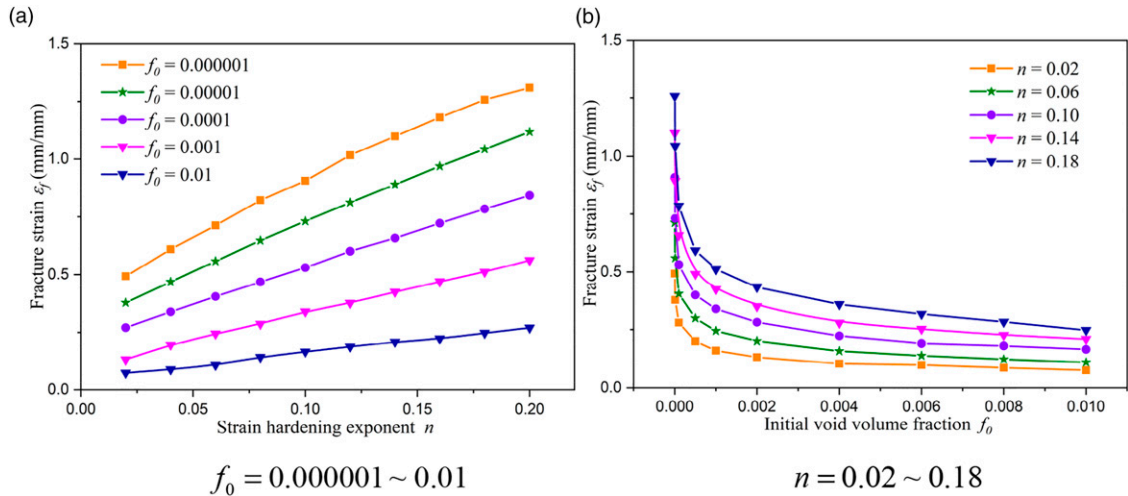

Figure 3. Relationship between the fracture strain and (a) plastic strain hardening exponent n and (b) initial void volume fraction f_0 of the "magic" notched tensile specimen.

For a given material the plastic hardening exponent n, the initial void volume fracture f_0 and fracture strain ε_f are uniquely correlated, the equation (5) can be rewritten as:

$$f_0 = f_0\left(\varepsilon_m, \varepsilon_f\right) \tag{6}$$

Various forms of equations have been used to fit the correlation data shown in Figure 3. It is found that the data shown in Figure 3 can be best fitted by the following equation:

$$f_0 = 1 / \exp\left(\alpha \cdot \varepsilon_f^2 + \beta \cdot \varepsilon_f + \gamma\right) \tag{7}$$

where α, β are functions of ε_m:

$$\alpha = -9.875 \cdot \exp(-20.01 \cdot \varepsilon_m) + 0.659 \tag{8}$$

$$\beta = 24.18 \cdot \exp(-13.39 \cdot \varepsilon_m) + 6.3 \tag{9}$$

$$\gamma = 17.7 \cdot \exp(-0.165 \cdot \varepsilon_m) - 14.73 \tag{10}$$

Figure 4 compares the initial void volume fraction calculated from equation (7) with the original data obtained
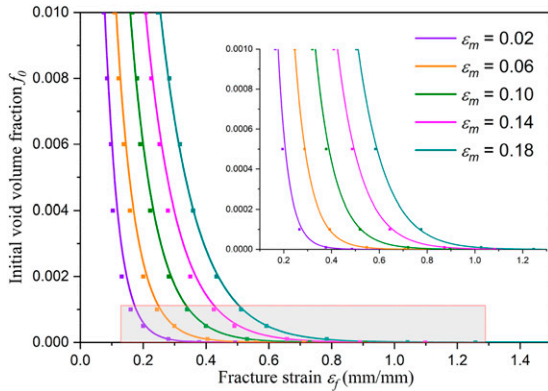

Figure 4. Comparison of the initial void volume fraction calculated from equation (7) and original data from Figure 3. Curves are from equation (7) and dots are the data from Figure 3.

from the finite element analyses. As can be observed from Figure 4, equation (7) fits the data points quite well. Even for f_0 in the range from 10^{-6} to 10^{-3}, a reasonable agreement is obtained. It should be noted that the applicability of equation (7) is limited to $\varepsilon_m = 0.02 \sim 0.2$, $\varepsilon_f = 0.07 \sim 1.3$.

Application to high strength steels and weld metal

The proposed equation (7) for inversely calculating the initial void volume fraction has been verified against three engineering materials with different plastic hardening ability and ductility. The three materials considered are: X80 pipe steel (marked as Specimen 1#), X80 girth weld (Specimen 2#) and 15CrMo steel (Specimen 3#). Specimen 1# and Specimen 2# were derived from a gas pipeline with a diameter of 1016 mm and a wall thickness of 18.4 mm. A total of 9 uniaxial tensile tests using the "magic" notch geometry have been conducted.

The experimental setup is displayed in Figure 5. The experiments were performed using a MTS 810-25 testing machine. The displacement-controlled mode was adopted, and loading speed was set to be 0.3 mm/min. The load-cross head displacement curves of the 9 specimens are presented in Figure 6. It can be seen that there are relatively small deviations in the load -displacement curves of the X80 steel and 15CrMo steel. As it can be expected, the results of the X80 girth weld (Specimen 2#) shows larger variation in both the load carrying capacity and fracture strain.

During the tensile testing, the deformations of notched specimens were captured every second by using an industrial digital camera. A python code was developed to retrieve the evolution of the minimum cross section diameter, from which the engineering stress and true strain of the notched tensile specimen can be evaluated. The engineering stress versus true strain curves of the 9 specimens are grouped into 3 figures shown in Figure 7. From these results, the corresponding fracture strain and strain
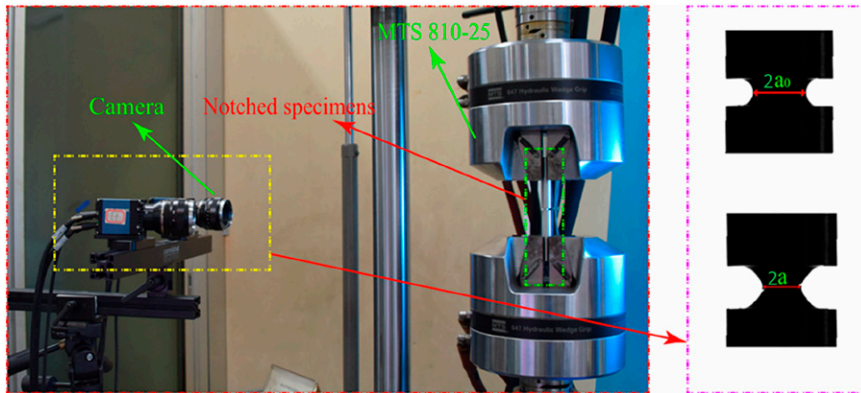

Figure 5. The experimental setup used for testing of the "magic" notched tensile specimens.
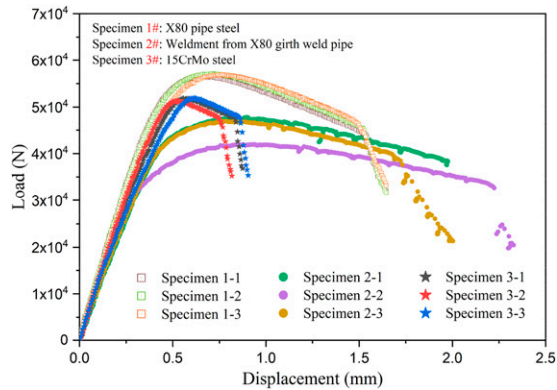
Figure 6. Load-cross head displacement curves of the 9 specimens made of three materials.

hardening exponent can be identified, and the effective initial void volume fraction is then calculated by applying equation (7). The measured yield stress, hardening exponent and fracture strain together with the calculated initial void volume fraction are summarized in Table 1. It is interesting to compare the X80 weld metal with the X80 base metal. The hardening ability of the weld metal is slightly higher than its base metal, however, the yield stress of the weld metal is significantly lower than that of the base metal and the weldment is a so-called undermatched weldment.

Table 1 shows the inversely calculated average initial void volume fractions for the three materials tested. The X80 steel has the smallest initial void volume fraction, with a mean value between 0.01% to 0.02%. It is interesting to observe from Table 1 and Figure 7 that although the fracture strain of the X80 weld metal is in the similar level of the X80 base metal, the average initial void volume fraction of the weld metal is much higher than, almost 3 times, those of the base metal. Figure 7 also shows that the fracture strain of the 15CrMo steel is the lowest among the three materials tested, and the average initial void volume fraction is approximately 15 times larger than the X80 steel. This finding indicates that the initial void volume fraction of a material is not solely determined by the ductility but is strongly dependent on the plastic strain hardening ability. For materials with identical fracture strain, the material with higher hardening ability will yield larger initial void volume fraction.

We note that the equation (7) was obtained based on the analysis of the ideal power-law hardening materials. It is interesting to verify that the application of the initial void volume fraction calculated from equation (7) will result in the same ductile fracture behaviour of the engineering materials. The measured yield stress and plastic strain hardening exponent and the initial void volume fraction shown in Table 1 have been taken as inputs to the finite element analyses, and the outputs from the finite element
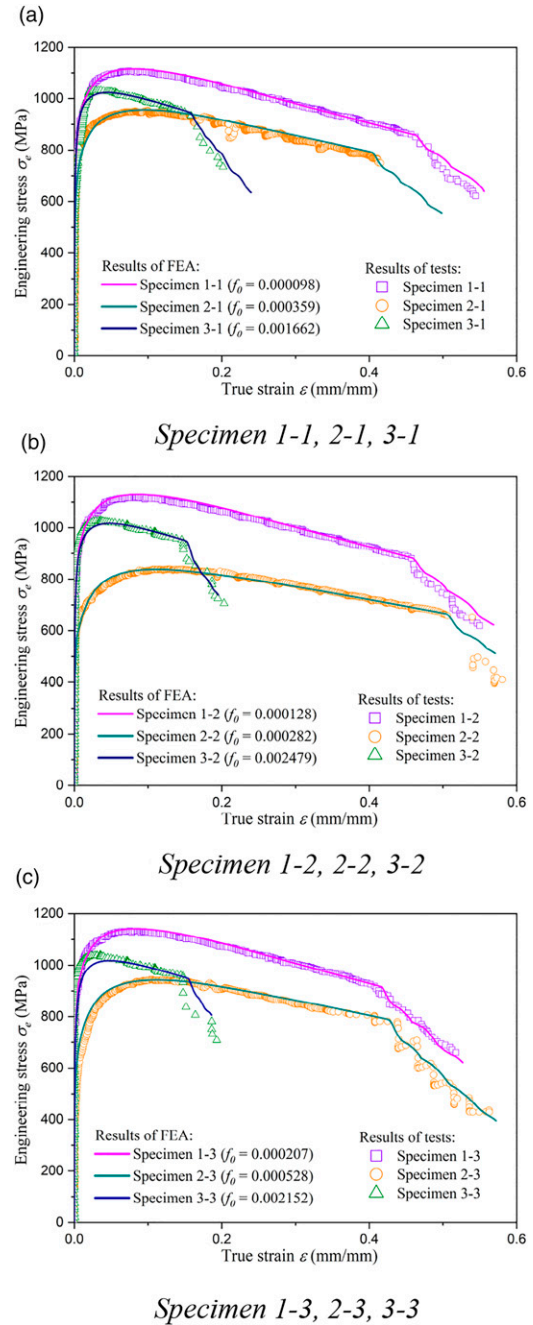

Figure 7. Comparison of the experimental engineering stress-true strain curves with the ones from finite element analyses using the data shown in Table 1. The points are from experiments and solid lines from finite element analyses using the initial void volume fraction fitted. (a) Specimen 1-1, 2-1, 3-1. (b) Specimen 1-2, 2-2, 3-2. (c) Specimen 1-3, 2-3, 3-3.

analyses have been compared with the experimental results in Figure 7. The comparison shows that the finite element results are in well accordance with the test results, especially the prediction of fracture strain is captured quite

Table 1. Mechanical properties and the inversely calculated initial void volume fraction.

	σ_0 (MPa)	n (ε_m)	ε_f	f_0 from equation (7)	Average f_0	Notes
Specimen 1-1	600	0.076	0.451	0.000098		
Specimen 1-2	595	0.083	0.455	0.000128	0.00014	X80 base metal
Specimen 1-3	610	0.079	0.406	0.000207		
Specimen 2-1	475	0.095	0.411	0.000359		
Specimen 2-2	370	0.121	0.506	0.000282	0.0004	X80 Weld metal
Specimen 2-3	430	0.117	0.438	0.000528		
Specimen 3-1	630	0.027	0.157	0.001662		
Specimen 3-2	620	0.032	0.146	0.002479	0.0021	15CrMo
Specimen 3-3	620	0.025	0.142	0.002152		

accurately. The good agreement confirms that the validity of equation (7).

Recommended procedures for identifying initial void volume fraction

In this work an explicit equation, equation (7), for inversely determining the initial void volume fraction for a given material is obtained. It has been shown that the equation possesses a good accuracy for the materials tested. Following recommended procedure is suggested.

(1) Prepare the "magic" notched tensile specimen as shown in Figure 1(a). It is particularly important that the notch geometry fulfils the requirement $a_0/R_0 = 2$. At least three parallel specimens should be prepared for each material.
(2) Perform uniaxial notched tensile tests. Both the applied load and the reduction of the minimum cross section diameter should be measured. Unlike the smooth tensile specimen, the elongation within a gauge length is not useful for the notched tensile specimen.
(3) Sketch the engineering stress-true strain curves of the notched tensile specimen ($\sigma_e - \varepsilon_t$) to identify the strain at the maximum load and the strain at fracture.
(4) Compute the initial void volume fraction f_0 with Equation (7) as a function of the hardening and fracture strain obtained in step (3).

When equation (7) is applied to the case where the volume of material of interest (weld metal or heat affected zone in a weldment) is limited, the zone size of the homogenous material to be tested should be as large as possible compared with the minimum cross section diameter $H/D_0 \geq 0.5$. When the material zone size is very small, the size of the notched tensile specimen can be scaled down accordingly to satisfy this geometrical requirement.

Discussion and conclusions

The "magic" notched tensile specimen has been shown previously to possess a special function, namely, the true stress-strain curve obtained from the tensile test using this special specimen can be directly converted into materials equivalent stress-strain curve without the need of performing a Bridgman correction. This study extends the function of the "magic" notched tensile specimen to determine the ductile damage parameter – the initial void volume fraction f_0. The CGM model has been applied to analyze the correlation between the predicted fracture behavior of the notched tensile specimen and its input parameter f_0. It is shown that the ductile fracture of the notched tensile specimen mainly depends on two parameters, the plastic strain hardening exponent and the initial void volume fraction. Because the fracture strain and plastic strain hardening exponent can be conveniently obtained from the strain-strain curve, an explicit equation to calculate the initial void volume fraction is proposed.

It is important to emphasize that the obtained the initial void volume fraction physically represents the effective initial void volume fraction of the tested material. The obtained effective initial void volume fraction ideally can be treated as a material ductility indicator, and transferred to the other cases with different stress triaxiality. However, the transferability may be material specific and remains to be experimentally verified in the near future. Only one notch geometry was considered in this study. Similar equations for other notched tensile specimens can be derived using the same procedure reported in this study. When the effective initial void volume fractions obtained from two notched tensile specimens differ significantly, question regarding the choice of the cluster void nucleation model should be raised. If that is the case, other void nucleation models, such as continuous void nucleation or statistical nucleation model may be considered [27]. There is only one parameter associated with the continuous void nucleation model. However, more than one parameter must be involved in the statistical void nucleation model. A good

advice is to fix as many parameters as possible and leave only one parameter to be identified.

In summary, based on the CGM model and by adopting a cluster void nucleation model and assuming that the void nucleation can be described by an effective initial void volume fraction, an explicit equation to calculate the effective initial void volume fraction using a special notched tensile specimen is presented. A recommended procedure for using the method is proposed. The method is particularly applicable to the cases where the size of the material zone of interest is limited, and it is impractical to machine the material to fabricate standard specimens for mechanical characterization. The method has been verified against three engineering materials including two types of high strength steels and one weld metal. It is expected that the method will facilitate the identification of damage parameters.

Highlights

- A method is proposed to explicitly calculate the effective initial void volume fraction from the strain at the maximum load and the strain at fracture of a specially designed notched tensile specimen.
- The method is well-suited for weldments where material volume of homogenous microstructure is limited.
- The proposed method has been experimentally verified by applying to three engineering materials including both high strength steels and an associated weld metal.
- This effective initial void volume fraction can facilitate the classification of deformation behavior of metallic materials.

Declaration of conflicting interests

The author(s) declared no potential conflicts of interest with respect to the research, authorship, and/or publication of this article.

ORCID iD

Zhiliang Zhang ⓘ https://orcid.org/0000-0002-9557-3455

References

Abendroth M and Kuna M (2006) Identification of ductile damage and fracture parameters from the small punch test using neural networks. *Engineering Fracture Mechanics* 73: 710–725.

Acharyya S and Dhar S (2008) A complete GTN model for prediction of ductile failure of pipe. *Journal of Materials Science* 43: 1897–1909.

Benzerga AA and Leblond J-B (2010) Ductile fracture by void growth to coalescence. In: Aref H and Giessen EVD (eds), *Advances in Applied Mechanics*. Elsevier.

Chen D, Li Y, Yang X, et al. (2021) Efficient parameters identification of a modified GTN model of ductile fracture using machine learning. *Engineering Fracture Mechanics* 245: 107535.

Chen Y and Lambert S (2003) Analysis of ductile tearing of pipeline-steel in single edge notch tension specimens. *International Journal of Fracture* 124: 179–199.

Dotta F and Ruggieri C (2004) Structural integrity assessments of high pressure pipelines with axial flaws using a micromechanics model. *International Journal of Pressure Vessels and Piping* 81: 761–770.

Gurson AL (1977) *Continuum Theory of Ductile Rupture by Void Nucleation and Growth: Part I—Yield Criteria and Flow Rules for Porous Ductile Media*.

Hadj Miloud M, Zidane I and Mendas M (2019) Coupled identification of the hardening behavior laws and Gurson–Tvergaard–Needleman damage parameters-Validation on tear test of 12NiCr6 CT specimen. *Frattura ed Integrità Strutturale* 13: 630–642.

Nonn A and Kalwa C (2012) Simulation of ductile crack propagation in high-strength pipeline steel using damage models. *International Pipeline Conference*. American Society of Mechanical Engineers, pp. 597–603.

Ouladbrahim A, Belaidi I, Khatir S, et al. (2021) Prediction of Gurson damage model parameters coupled with hardening law identification of steel X70 pipeline using neural network. *Metals and Materials International* 28: 370–384.

Qiang B and Wang X (2019) Ductile crack growth behaviors at different locations of a weld joint for an X80 pipeline steel: a numerical investigation using GTN models. *Engineering Fracture Mechanics* 213: 264–279.

Sarzosa DF, Verstraete M, Hertelé S, et al. (2016) Numerical simulation of ductile crack growth in medium wide plate specimens using 3-D computational cells. *Engineering Fracture Mechanics* 168: 26–45.

Scheider I, Nonn A, Völling A, et al. (2014) A damage mechanics based evaluation of dynamic fracture resistance in gas pipelines. *Procedia Materials Science* 3: 1956–1964.

Seupel A, Hütter G and Kuna M (2020) On the identification and uniqueness of constitutive parameters for a non-local GTN-model. *Engineering Fracture Mechanics* 229: 106817.

Springmann M and Kuna M (2005) Identification of material parameters of the Gurson–Tvergaard–Needleman model by combined experimental and numerical techniques. *Computational Materials Science* 33: 501–509.

Sun D-Z, Siegele D, Voss B, et al. (1989) Application of local damage models to the numerical analysis of ductile rupture. *Fatigue and Fracture of Engineering Materials and Structures* 12: 201–212.

Tanguy B and Besson J (2002) An extension of the Rousselier model to viscoplastic temperature dependent materials. *International Journal of Fracture* 116: 81–101.

Tanguy B, Besson J, Piques R, et al. (2005) Ductile to brittle transition of an A508 steel characterized by Charpy impact test: part II: modeling of the Charpy transition curve. *Engineering Fracture Mechanics* 72: 413–434.

Thomason P (1990) *Ductile Fracture of Metals*. Ductile Fracture of MetalsUK: Pergamon Press plc, 1990, p. 219.

Tu S, Ren X, He J, et al. (2018) A method for determining material's equivalent stress-strain curve with any axisymmetric notched tensile specimens without Bridgman correction. *International Journal of Mechanical Sciences* 135: 656–667.

Tu S, Ren X, He J, et al. (2019) Experimental measurement of temperature-dependent equivalent stress-strain curves of a 420 MPa structural steel with axisymmetric notched tensile specimens. *Engineering Failure Analysis* 100: 312–321.

Tu S, Ren X, He J, et al. (2020) Stress–strain curves of metallic materials and post-necking strain hardening characterization: a review. *Fatigue and Fracture of Engineering Materials and Structures* 43: 3–19.

Tu S, Ren X, Nyhus B, et al. (2017) A special notched tensile specimen to determine the flow stress-strain curve of hardening materials without applying the Bridgman correction. *Engineering Fracture Mechanics* 179: 225–239.

Tvergaard V (1981) Influence of voids on shear band instabilities under plane strain conditions. *International Journal of Fracture* 17: 389–407.

Tvergaard V (1982) On localization in ductile materials containing spherical voids. *International Journal of Fracture* 18: 237–252.

Tvergaard V and Needleman A (1984) Analysis of the cup-cone fracture in a round tensile bar. *Acta Metallurgica* 32: 157–169.

Zhang Y, Lorentz E and Besson J (2018) Ductile damage modelling with locking-free regularised GTN model. *International Journal for Numerical Methods in Engineering* 113: 1871–1903.

Zhang Z (1995a) Explicit consistent tangent moduli with a return mapping algorithm for pressure-dependent elastoplasticity models. *Computer Methods in Applied Mechanics and Engineering* 121: 29–44.

Zhang Z (1995b) On the accuracies of numerical integration algorithms for Gurson-based pressure-dependent elasto-plastic constitutive models. *Computer Methods in Applied Mechanics and Engineering* 121: 15–28.

Zhang ZL (1996) A sensitivity analysis of material parameters for the Gurson constitutive model. *Fatigue and Fracture of Engineering Materials and Structures* 19: 561–570.

Zhang Z, Hauge M, Thaulow C, et al. (2002) A notched cross weld tensile testing method for determining true stress–strain curves for weldments. *Engineering Fracture Mechanics* 69: 353–366.

Zhang ZL and Niemi E (1995) A new failure criterion for the Gurson-Tvergaard dilational constitutive model. *International Journal of Fracture* 70: 321–334.

Zhang ZL and Niemi E (1995a) A class of generalized mid-point algorithms for the Gurson–Tvergaard material model. *International Journal for Numerical Methods in Engineering* 38: 2033–2053.

Zhang Z, Thaulow C and Ødegård J (2000) A complete Gurson model approach for ductile fracture. *Engineering Fracture Mechanics* 67: 155–168.

Zhang ZL and Niemi E (1994b) Studies on the ductility predictions by different local failure criteria. *Engineering Fracture Mechanics* 48: 529–540.

Appendix

Notation

a_0	Radius of the minimum cross section of a notched specimen
D	Diameter of the minimum cross section
D_0	Outer diameter of the notched tensile specimen
E	Young's modulus
f	Current void volume fraction
f_0	Initial void volume fraction
f_c	Critical void volume fraction
f_F	Void volume fraction at failure
H	Width of the weld metal
L	Length of the notched tensile specimen
l_0	Uniform element size at the minimum cross ection
n	Plastic strain hardening exponent
P_f	Fracture load
P_m	Maximum load in a notched tensile test
q	The von Mises equivalent stress
q_1, q_2	Tvergaard constants for modifying the Gurson model
R_0	Notch radius
v	Poisson ratio
σ_0	Yield stress of the material
σ_h	Mean stress
σ_e	Average engineering stress of the notched tensile specimen defined as the tensile load divided by the initial minimum cross-sectional area
σ_m	Average engineering stress at the maximum load

σ_t Average true stress of the notched tensile specimen defined as the tensile load divided by the current minimum cross-sectional area

$\bar{\sigma}$ Flow stress of the material

ε_0 Yield strain of the material

ε_f Fracture strain - true strain corresponding to P_f

ε_m Strain at the maximum load - true strain corresponding to P_m

ε_p Equivalent plastic strain of the material

ε_t Average true strain calculated from the reduction of the minimum cross-sectional area

α, β Fitted functions of ε_m